Improvement of Microscopic MR Imaging of Amyloid Plaques with Targeting and Non-Targeting Contrast Agents

Alexandra Petiet[1,2,3] and Marc Dhenain[1,2,3*]

[1]*CNRS, URA 2210, 18 Route du Panorama, 92265 Fontenay aux Roses, France*

[2]*CEA, I2BM, MIRCen, 18 Route du Panorama, 92265 Fontenay aux Roses, France*

[3]*CEA, I2BM, Neurospin, CEA Saclay, Bat. 145, 91191 Gif-sur-Yvette, France*

Abstract: Overaccumulation of β–amyloid in the brain is believed to be a primary event in the development of Alzheimer's disease (AD). This amyloid is the target of drugs currently under development for the treatment of AD, which makes imaging amyloid plaques essential. Magnetic resonance imaging (MRI) has the resolution required to resolve these microscopic lesions (~ 50 μm). In the absence of any contrast agent, the source of MR contrast in the amyloid plaques comes from the accumulation of iron, which shows as hypointense spots in T_2, T_2* or susceptibility-weighted images. Iron deposition in the brain is an age-related phenomenon and its accumulation occurs mainly in iron-rich regions. For plaques weakly loaded with iron, whose detection is much more challenging, the use of exogenous contrast agents (CA) becomes necessary. This article describes (1) targeted CAs made of a paramagnetic element like Gadolinium linked to a pharmacophore that targets amyloid, and (2) non-targeted CAs, an alternative to enhance amyloid plaque visualization. A background on CAs is also presented, and current issues related to contrast-enhanced MR imaging, including difficulties in delivering these agents across the blood-brain barrier, are also discussed.

Keywords: Alzheimer, amyloid plaques, MRI, contrast agent, passive staining, Gadolinium.

INTRODUCTION

Alzheimer's disease (AD) is the most common type of neurodegenerative diseases with 4.6 million new cases per year in the world. This disease is neuropathologically characterized by two microscopic lesions: the intracellular formation of neurofibrillary tangles and the extracellular deposition of aggregated β-amyloid (Aβ) peptides in amyloid (or senile) plaques. Amyloid peptides arise from the abnormal metabolism of the transmembrane amyloid precursor protein (APP) that is cleaved by the γ- and β-secretase enzymes, releasing the neurotoxic Aβ fragments. Amyloid plaques are believed to occur in the brain up to 20 years before the occurrence of the clinical diagnosis of AD [1]. According to the amyloid cascade hypothesis, these Aβ peptides are at the origin of a cascade of events [2] that lead to neuronal dysfunctioning, dendritic and neuronal losses, and to cerebral atrophy throughout the progression of the disease [3]. The critical role of amyloidosis in the development of AD has led several therapeutic strategies to target its reduction in the brain [4]. The ability to image amyloid plaques in humans and in animal models of amyloidosis is thus critical to follow the effects of new drugs in development.

In humans, amyloid plaques can be imaged with positron emission tomography (PET) by using dedicated agents like the Pittsburgh compound B (PiB [5, 6]). However, its short period of life (half-life time of 20 minutes for ^{11}C) does not make PiB suitable for routine use in a clinical environment at this time, but ongoing research develops agents with longer half-lives [7]. The ability to image amyloid plaques in animals is also critical to evaluate new treatments against AD at a preclinical stage. To date, PET agents do not enable the detection of amyloid plaques in mouse models of AD [8, 9]. Also, even when new contrast agents (CA) will enable plaque detection, the low spatial resolution of PET will remain an issue to detect them in small animals, where important partial volume effects are introduced. The high resolution achievable by MRI allows direct detection of amyloid lesions both in humans and in animals. Today, in the context of AD pathology, MRI is used in humans to mainly evaluate cerebral atrophy in hippocampal and temporal regions as an index of disease occurrence and progression [3].

The first attempts to detect amyloid plaques by MR were performed on human post-mortem brain samples. It was first shown that amyloid plaques can be detected on T_2*-weighted (T_2*w) and on diffusion-weighted images [10]. However, further studies suggested that senile plaques do not always cause susceptibility effects in T_2*w images [11]. More recent studies showed that susceptibility-weighted images (SWI) can help detect ex-vivo [12] or in-vivo amyloid plaques in humans [13]. The ability to detect plaques by MRI seems to be related to their iron content [14]. Similarly, studies in mice also showed that some plaques can be detected as dark spots on ex-vivo [15-17] or *in-vivo* [17, 18] T_2, T_2* or SWI images [19]. The ability to detect them also seems to be highly dependant on the iron load within the plaques. However, several studies emphasized the heterogeneity of amyloid deposits. First, thalamic plaques were shown to accumulate much more iron and calcium than hippocampal or cortical plaques [20]. This accumulation induces strong T_2 and

*Address correspondence to this author at the MIRCen, CEA/CNRS URA 2210, 18 Route du Panorama, 92265 Fontenay aux Roses, France; Tel: +33 1 46 54 81 92; Fax: +33 1 46 54 84 51; E-mail: marc.dhenain@cea.fr

1573-4056/11 $58.00+.00

T_2* effects in the thalamic plaques that can thus be detected as large hypointense spots on T_2 or T_2* images [16, 20-22]. Second, young AD animals present small plaques that do not accumulate as much iron as old animals, especially in cortical and hippocampal regions [23]. The scope of this manuscript is to review the use of MR contrast agents to overcome difficulties related to the heterogeneity of plaques and to facilitate their detection by MRI.

1. CONTRAST ENHANCEMENT PRINCIPLES

1.1. Molecular Basis of Relaxation Enhancement

The principal source of MR contrast relies on differences in tissue relaxation time, either inherent to the tissue (endogenous contrast), introduced to the tissue (exogenous contrast) or caused by magnetic field perturbations. After excitation by a radiofrequency pulse, the water protons from different tissues differentially come back to equilibrium following a spin-lattice relaxation time T_1 and a spin-spin relaxation time T_2. The different relaxation times between various tissues provide the contrast within MR images [24]. When the spontaneous contrast between tissues is not sufficient, one can use CAs as exogenous contrast enhancers [24]. The signal enhancement produced by CAs depends on their longitudinal (r1) and transverse (r2) relaxivities (expressed in $mmol^{-1}\ s^{-1}$), which is defined as the increase of the nuclear relaxation rate (the inverse of the relaxation time) of water protons produced by 1 mmol per liter of CA.

The effect of a contrast agent modifying T_1 relaxation times is described by the following equation [25]:

$$R1 = R1_0 + r_1[C]$$

Where R1 is the relaxation rate of the tissue with the paramagnetic agent, $R1_0$ is the relaxation rate of the tissue in the absence of CA, r_1 is the relaxivity of the agent, and C is the concentration of the agent. The same equation can be derived for T_2 relaxation time.

To be efficient, relaxation enhancers must possess two properties: they must come to the vicinity of water molecules and they must be able to magnetically interact with hydrogen nuclei. Paramagnetic molecules used as CAs have a large number of unpaired electrons and a long electronic relaxation time. Electrons have an intrinsic magnetic dipole moment (much larger than the nuclear moment) due to their electronic spin. As a consequence, they can interact with the nuclear spins through electron-nuclear dipolar interactions – they increase the rate of transfer of energy to the lattice, which shortens the T_1 relaxation times of the tissues. These interactions are generally described within three different molecular environments: (1) the bulk water where the distance between the water molecules and the paramagnetic centers is large so the molecular interactions are weak, (2) the inner sphere where the distance between the water molecules and the paramagnetic centers is the smallest so the water molecules bind closely to the paramagnetic agent, and (3) the outer sphere water – the transition region between the bulk water and the inner sphere where only water molecules that diffuse close enough to the paramagnetic centers interact with them. The relaxation enhancement parameters are described by the Solomon-Bloembergen-Morgan (SBM) theory [26-28]. According to this theory, the relaxivity that characterizes a CA is equal to the sum of the relaxivities in all three molecular regions. However, the inner and outer spheres are considered to provide the major contributions to the relaxivity, with the dominant effect coming from the inner sphere, and a non-negligible effect (~ 40%) coming from the outer sphere [29].

1.2. Paramagnetic and Superparamagnetic Contrast Agents

The use of paramagnetic molecules as MR CAs was described by Mendonça-Dias *et al*. in 1983 [30]. The Gadolinium (Gd) element is a lanthanide with 7 unpaired electrons and a high magnetic moment (7.6 magnetons). These properties make it an element of choice for relaxation enhancement of protons in biological tissues. However, Gd must be chelated to be used in biological samples to remove the high toxicity of its free form [31]. A number of Gd chelates have been developed and commercialized, and they are widely used as CAs in clinical settings (e.g. Gd-DTPA, Magnevist®, Schering; Gd-DOTA, Dotarem®, Guerbet; Gd-DTPA-BMA, Omniscan®, Amersham; Gd-HP-DO3A, ProHance®, Bracco; Gd-DTPA-BMEA, Optimark®, Mallinkrodt; Gd-DO3A-Butriol, Gadovist®, Schering). Other paramagnetic agents based on other lanthanides, such as Dysprosium, have also been proposed and could be a good alternative to Gd agents especially at high magnetic fields [32].

Superparamagnetic agents have a much larger magnetic susceptibility than paramagnetic agents. They are made of iron particles of various sizes and properties: small particles of iron oxide (SPIO, diameter 50-150 nm), ultra small particles of iron oxide (USPIO, diameter 20-40 nm) or even smaller particles such as monocrystalline iron oxide nanoparticles (MION, diameter 1-10 nm). These agents induce strong local magnetic field variations that significantly reduce T_2 relaxation times and therefore reduce the signal in MR images. Their size varies widely and determines their physicochemical and pharmacokinetic properties, and therefore also determines their field of application [33]. For example, SPIOs are used for liver, spleen or lymph nodes imaging and USPIOs, due to their very small size and longer blood half-life, can be used for MR angiography, perfusion or functional imaging.

1.3. Effect of Contrast Agents on Tissue Relaxation Times, Signal and Contrast Enhancement

According to the SBM theory described previously, when a paramagnetic molecule, such as a Gd chelate, comes to the vicinity of water protons, it perturbs their magnetic environment at the microscopic level such that proton relaxation is accelerated. This phenomenon leads to a T_1 relaxation shortening in the tissue, which in turn leads to an increased T_1 signal. If CA administration leads to an increased T_1 difference between adjacent tissues, then the contrast between those tissues increases. Fig. (**1**) illustrates T_1 shortening and contrast enhancement (at 7 Tesla) for two adjacent tissues (the hippocampus and the corpus callosum) without and with a non-targeted CA. In this example, the contrast agent modifies the T_1 in both structures. In the hippocampus: T_1 without CA = 1580 ms while T_1 with CA = 165 ms. In the corpus callosum: T_1 without CA = 1440 ms while T_1 with CA = 210

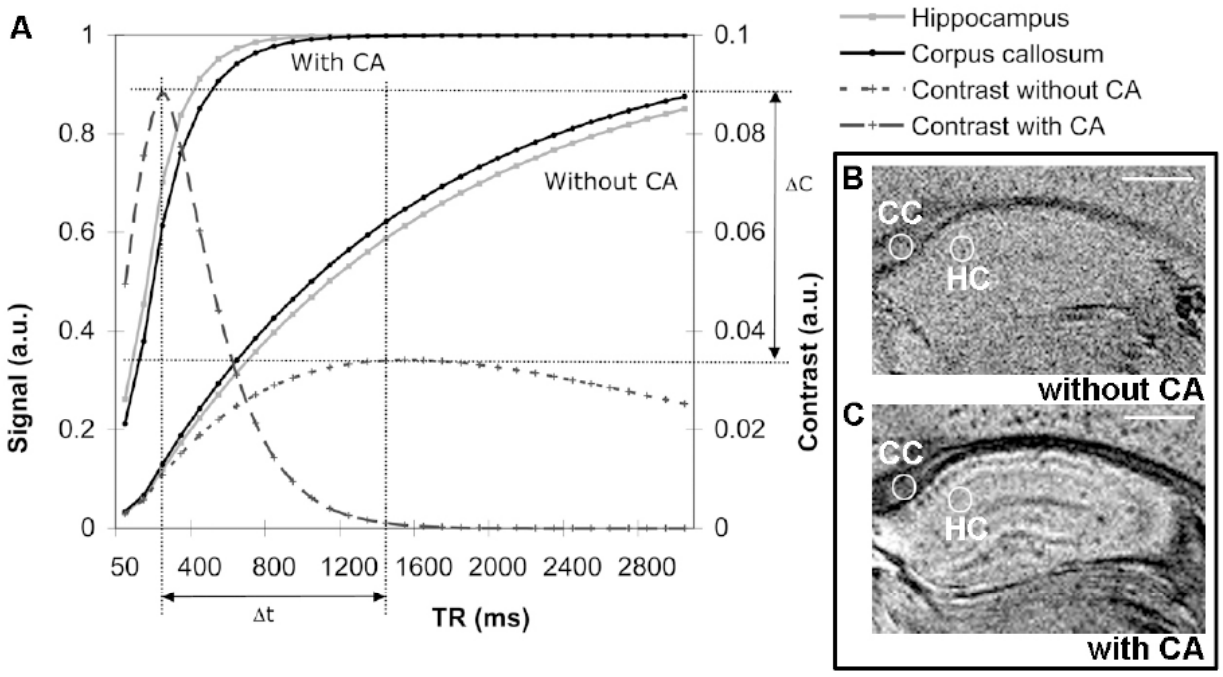

Fig. (1). Gd effect on T_1 relaxation time and contrast enhancement. Two T_1 recovery curves (signal recovery as a function of repetition time) are plotted for two adjacent tissues (the hippocampus (HC) and the corpus callosum (CC)), with and without a contrast agent (CA). The left y axis represents the signal intensity within a particular tissue while the right y axis represents the contrast (i.e. signal difference) of the two tissues. In this example, the contrast between the hippocampus and the corpus callosum increases by a factor of 2.5 (from ~ 0.035 to 0.09) after addition of a CA. The maximum contrast occurs earlier in time with a CA (maximum contrast at a repetition time (TR) = 200 ms) relative to the case without CA (maximum contrast at TR = 1500 ms), which means that faster acquisitions are possible. Δt = time difference between the maximum contrast obtained without CA and the maximum contrast obtained with CA (i.e. time gain); ΔC = contrast difference between the case without CA and the case with CA (i.e. contrast enhancement).

The relaxation curves (A) were measured at 7T by using a 2D turbo spin-echo sequence (RARE; TR = 338, 500, 1000, 2000, 4000 and 8000 ms, TE = 8.3 ms, acquisition time = 12 min for the T_1 measurements; TR = 8000 ms, TE = 7 – 105 ms with 14 ms increments, acquisition time = 6 min for the T_2 measurements).

The images B-C were acquired at very high resolution with a gradient-echo sequence (FLASH, TR/TE = 100/19.4 ms, $\alpha = 25^{\circ}$, resolution = 23 x 23 x 90 μm^3, acquisition time = 12 hrs. Scale bars = 500 μm (data from [34]).

ms (data from [34]). In this example, introducing a CA shortens T_1 of the hippocampus by ten times and shortens T_1 of the corpus callosum by seven times (Fig. (**1**) - left axis). This T_1 shortening translates into a contrast (i.e. signal difference) increase between the two tissues by over a factor of 2.5 (Fig. (**1**) - right axis). In addition, because of those relaxation time shortenings, the maximum contrast is reached earlier in time (Δt in Fig. (**1**)): it is reached at TR = 1500 ms without a CA, and at TR = 200 ms with a CA. This represents a significant gain in acquisition time by a factor of 8.

Similarly, non-targeted contrast agents might modify differentially the T_1 (or T_2) of plaques and adjacent parenchyma thus leading to an enhanced contrast between plaques and adjacent parenchyma at shorter TR. On the other side, targeted contrast agents are expected to specifically modify the relaxation time of the targeted structure, for example the amyloid plaque. In this case, the T_1 (and T_2) difference between the plaques and cortical parenchyma is also increased, which leads to a better detection of amyloid plaques.

2. AMYLOID PLAQUE IMAGING WITH TARGETED CONTRAST AGENTS

Fig. (**2**) shows typical images illustrating amyloid plaque detection using a targeted contrast agent (such as Gd-DTPA-Aβ1-40 or Gd-DTPA-Aβ1-30) (from [35]). Such agents allow a twofold increase of the number of detected amyloid plaques in MR images (see Fig. 2 and 3 in [36]). A larger increase of the number of plaques detected was recently shown in T_1w MR images of histological sections incubated with Gd-DOTA linked to an antibody targeting the amyloid plaques (pF(ab′)24.1) [37]. The enhanced detection of amyloid plaques with contrast agents is related to the increased contrast-to-noise ratio (CNR) between plaques and adjacent tissues. This has been quantified in a study by Poduslo et al. that showed a twofold and a ninefold increase of the CNR between plaques and adjacent tissues on T_2w and T_1w images, respectively, following administration of putrescine–Gd–amyloid-β peptide [38].

To be efficient, the targeted contrast agents that are used to detect in-vivo Aβ plaques must (1) be highly stable, (2) have a magnetic effect on tissues, (3) bind specifically to plaques, (4) cross the blood-brain barrier (BBB), and (5) diffuse from their site of entrance in the brain to the targeted plaques. Different approaches have been investigated to satisfy these properties.

The magnetic effect of these agents can be achieved by binding a paramagnetic agent like Gd, or a superparamagnetic agent like a MION to them [38, 39]. Gd-based agents

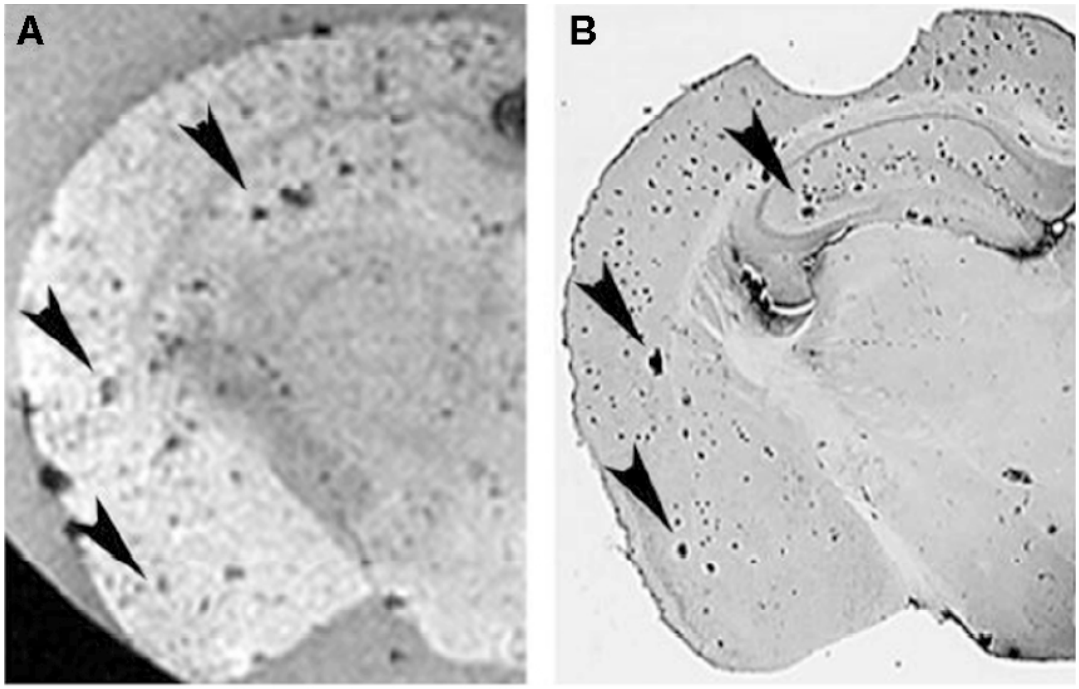

Fig. (2). Ex-vivo T_2*w image (**A**) and matched histology section (**B**) showing amyloid plaque detection (arrowheads) after carotid injection of Gd-DTPA-Aβ1-40. TR/TE = 500/10 ms, FA = 55º, in-plane resolution = 59 x 59 μm^2, slice thickness = 500 μm, acquisition time = 35 min. From [35].

positively enhance the signal associated to amyloid plaques in T_1w images, but contrast enhancement is stronger in T_2w or T_2*w images due to susceptibility effects from the plaques and associated CA [39]. MION-based agents are even more sensitive than Gd agents because their effect on T_2 or T_2* is stronger. However, despite an apparent increased sensitivity, MION-based constructs lead to greater individual variability to detect Aβ plaques. This is likely due to the large size of the MION-based construct and the reduced corresponding BBB permeability, even in the presence of a compound, such as mannitol, that opens the BBB. A recent study has investigated Dysprosium (Dy) as a Gd substitute. It showed a stronger T_2 and T_2* effect for the Dy-based amyloid plaque labeling agents as compared to Gd based agents [40]. Dysprosium agents could thus be used as an alternative to Gd and MION-based agents, especially at high magnetic fields.

The binding affinity of the targeted agent to endogenous Aβ can be achieved by using pharmacophores such as Aβ ligands. Indeed, exogenous Aβ has the property to aggregate with endogenous Aβ within amyloid deposits. This property was first shown in in-vitro studies by using radiolabeled Aβ [41]. In-vivo studies based on this concept have shown that Aβ1-40 peptide tagged with MR CAs can detect amyloid plaques in AD mice [38, 39]. The MR image shows a large number of plaques compared to the matched histology section. However, full-length Aβ1-40 fragments can induce amyloid plaque formation, which does not make them suitable targeting peptides in pharmacological trials. Alternatively, Aβ1-30 truncated fragments are less toxic and are used for their therapeutic potential as a vaccine [42]. These fragments have a high Aβ affinity but do not promote Aβ aggregates and they are cleared from the body within 2 weeks [36]. For ultimate human applications, Aβ homologous peptides will have to be developed with high solubility and reduced fibrillogenic and amyloidogenic potential. Other strategies use agents based on targeting monoclonal antibodies raised against amyloid proteins. In-vitro studies showed that polyamine-modified $F(ab')_2$4.1 antibody fragment of the monoclonal IgG4.1 raised against Aβ40 human protein have a high Aβ binding affinity [43]. This agent, coupled with Gd-DTPA, was used to detect amyloid in mice and showed improved detection on T_1w and T_2w images [37, 43]. The clearance of such agent is also relatively quick as its plasmatic concentration is low 6 hours after injection [37].

Another difficulty in targeting amyloid plaques comes from the ability to bring the CA to their vicinity. Several strategies have been investigated to pass molecules through the BBB. The BBB can transiently be opened by co-injecting a hyperosmotic solution of mannitol [39], however, this solution is toxic. An alternative way to pass a molecule through the BBB is by increasing its permeability with naturally occurring polyamines like putrescine, spermidine or spermine. These polyamines, when covalently attached in-vitro to proteins, were shown to significantly increase the protein permeability coefficient-surface area product [44]. More specifically, putrescine bound to Aβ1-40 was shown to increase in-vivo BBB permeability in mice [38]. In the future, new strategies will have to be defined to bring the CA close to the amyloid plaques through the BBB. Today, popular approaches rely on the use of ultrasounds and microbubbles to open the BBB [45-48]. Other methods used to open the BBB, such as the use of lipid-soluble agents, proteins (carriers) or association of CAs with proteins that can be taken up by specific receptor-mediated endocytosis and transcytosis mechanisms or by adsorptive-mediated endocytosis [49, 50], will also need to be explored.

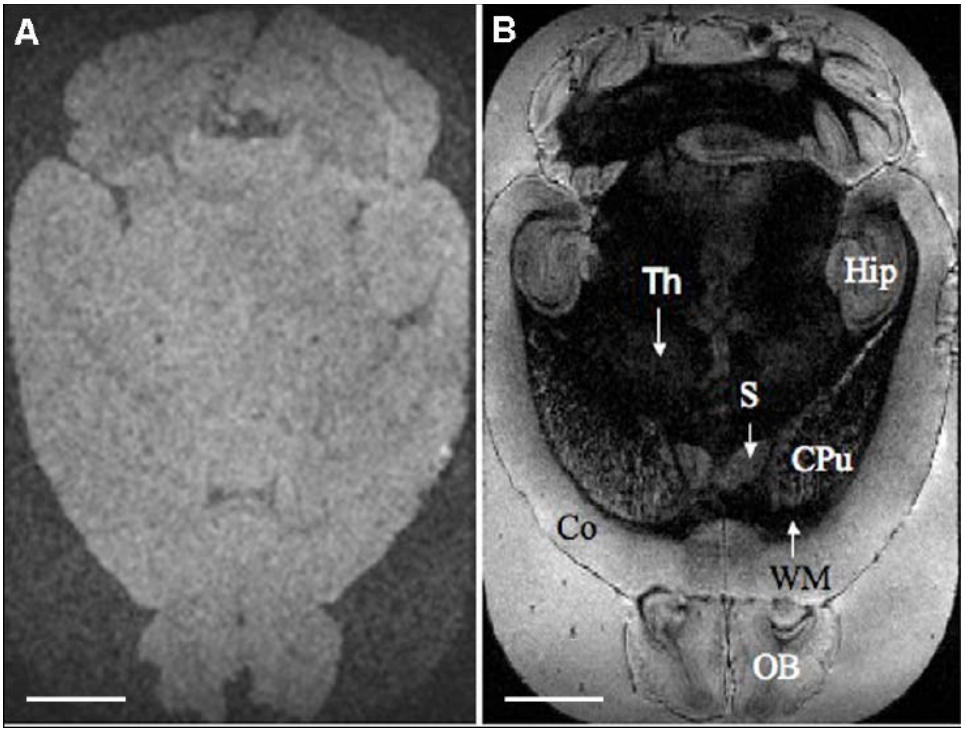

Fig. (3). MR images of mouse brains before (**A**) and after (**B**) staining with a Gd CA. The SNR and CNR are greatly increased after passive staining. Co: cortex; CPu; caudate putamen (striatum); Hip: hippocampus; OB: olfactory bulb; S: septum; Th: thalamus; WM: white matter. The two images were recorded with the same imaging parameters: 3D gradient-echo sequence, TR/TE = 100 / 20 ms, alpha = 90°, resolution = 63 x 47 x 59 μm^3 zero-filled to provide a digital resolution of 31.5 x 23.5 x 29.5 μm^3) Scale bars = 2 mm. Modified from [52].

3. AMYLOID PLAQUE IMAGING WITH NON-TARGETED CONTRAST AGENTS

3.1. Principle of Active and Passive Staining

Most of the first developments regarding contrast-enhanced amyloid plaque imaging by MRI were based on the use of targeted agents. However, the use of these agents is limited mainly by their availability and their toxicity. As an alternative, non-targeted Gd-based agents can be used and have the advantage of being clinically validated, widely available and non-toxic. Non-targeted agents were broadly used in the context of microscopic MR imaging to stain brain tissues. The use of non-targeted Gd CAs in rodents was first introduced by Johnson *et al*. in 2002 [51]. In their protocol, animals were perfused with a CA in conjunction with a fixing agent such as formalin. The Gd agent diffused from the vascular system into the soft tissues and increased the signal and contrast within tissues. This protocol was called "active staining". Later, Dhenain *et al.* developed a "passive staining" protocol [52, 53] based on the immersion of excised brain samples in a Gd solution (Fig. (**3**)). In this technique, the CA passively diffuses into the tissue due to concentration gradients, and significantly increases the contrast between tissues, for example the contrast between the cortex and white matter. This protocol can be used for already fixed samples, fresh tissue or concomitantly with a fixing agent, which makes this technique flexible.

3.2. Applications in Post-Mortem Biology

Staining tissue samples with a non-targeted Gd CA has been used in a wide variety of applications. In addition to increasing the contrast, the method increases the signal-to-noise ratio (SNR) in some brain tissues by a factor of 3 or more [34]. This SNR gain is similar to that obtained by tripling the strength of the magnetic field. Thanks to this signal gain and also to an improved contrast between tissues, very high-resolution images (down to 20 μm) showing exquisite detail can be recorded. Examples include the use of Gd CAs for MR histology of whole mice [54] or excised brains [55]; mouse embryo atlasing [56, 57]; mouse brain atlasing or for the evaluation of cerebral pathologies [53, 58]. In addition to using Gd CAs as T_1w contrast enhancers, they have also been used to enhance SNR in diffusion tensor imaging (DTI) sequences for high-resolution acquisitions of post-mortem non-human primate brains [59] or developing rabbit brains [60]. These examples illustrate the broad applications of tissue staining with non-specific Gd-based CAs due to their availability in laboratories.

3.3. Applications of Passive Staining for Amyloid Plaque Imaging

Our group has developed protocols based on the use of non-targeted Gd chelates (e.g. gadoterate meglumine) to improve plaque detection [52]. The rationale is based on the hydrophilic property of these Gd chelates [61] which do not come to the vicinity of hydrophobic structures like β-sheeted amyloid plaques. Thus in AD brains, they enhance the parenchymal signal and not the signal of plaques, thereby increasing the contrast between the two structures.

One of the limiting factors in recording high-resolution MR images is the loss of SNR that occurs when the resolution of the image increases. The signal gain due to the CA

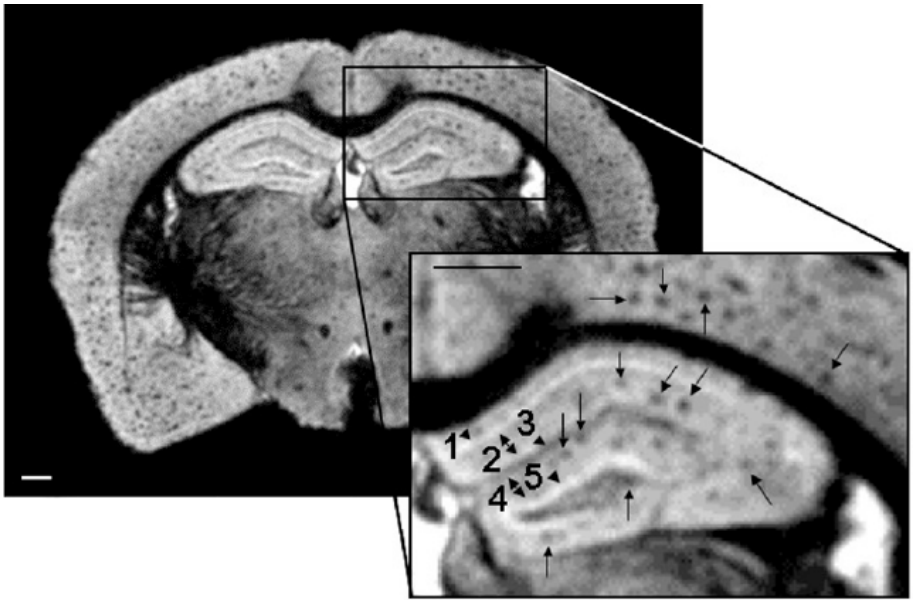

Fig. (4). Amyloid plaque detection with passive staining in a 12-month old APP/PS1 ΔE9 mouse. The formalin perfusion-fixed brain was immersed in a solution of phosphate buffered saline and Gd for at least 24 hours. The significant gain in signal and contrast allows high-resolution overnight imaging at 23 μm in plane. Gross anatomical structures of the brain as well as cellular and molecular layers can clearly be identified (numbered arrowheads and arrows): (1) pyramidal cell layer of the hippocampus; (2) lacunosum moleculare layer of the hippocampus; (3) hippocampal fissure; (4) molecular layer of the dendate gyrus; (5) granular layer of the dendate gyrus. Many individual plaques are visible (some are identified with arrows). Scale bars = 500 μm.

can thus be used to increase the resolution of the image while maintaining a good SNR. Thus, thanks to better resolution and contrast provided by passive staining, cellular layers within brain regions can be resolved, such as those in the hippocampus or even individual amyloid plaques of about 50 μm (Fig. (**4**)). With this level of detail, it is possible to follow disease progression through amyloid plaque increased load. More interestingly, recent data suggest that such protocols can be applied to in-vivo imaging of amyloid plaques after intracerebroventricular injection of a CA [34]. In addition, non-specific Gd chelates are well suited for longitudinal studies in animal models because they are not expected to interfere with endogenous amyloid and promote amyloidosis unlike agents made of Aβ fragments.

CONCLUSIONS

Imaging amyloid plaques is one of the current challenges of MRI. In animals, an obvious application of such imaging protocols would be to assess amyloid load and to be able to follow the effects of anti-amyloid treatments at a preclinical stage. Without contrast agents, large plaques are MR detectable due to their endogenous iron content in old animals, but smaller and earlier plaques require the use of contrast agents. Several protocols based on targeted or non-targeted CAs are currently able to routinely detect plaques. Targeted CAs have shown very good plaque enhancement. Their main advantage is that they can specifically target amyloid plaques. The first generation of agents was based on amyloid peptides and thus risked to accelerate amyloid plaque formation. New agents recently developed are based on Aβ derivatives or antibodies that do not induce Aβ plaque formation. However, the drawback of these agents is that they are currently only available in few laboratories and they are not used on a routine basis. In contrast, non-targeted CAs are easy to use and they have the potential to become widely used for preclinical MR imaging of amyloid plaques. They can be administered directly into the cerebral ventricles for in-vivo imaging [34], and extracted brains can simply be soaked in a Gd solution to yield significant plaque enhancement. Future developments will lead to products that cross the BBB. The effect of such products on the amyloid pathology will have to be assessed to ensure that their administration does not modulate the amyloid load.

The ability to image amyloid plaques thanks to MR contrast agents also has potential applications in humans to diagnose AD and to follow-up therapies. However, today, the first trials of in-vivo imaging of amyloid plaques in humans were based on spontaneous contrast but they provided controversial results. We expect that future trends in humans will include discoveries of new CAs that can safely be administered to enable plaque detection, but the same problems as in animals (stability, specificity of the plaque detection, BBB opening) will thus have to be addressed as well as their toxic effects.

ACKNOWLEDGEMENTS

Our work was supported by the France-Alzheimer association, the National Foundation for Alzheimer's Disease and Related Disorders, and the NIH (R01-AG020197).

REFERENCES

[1] Jack CR, Jr., Lowe VJ, Weigand SD, *et al.* Serial PIB and MRI in normal, mild cognitive impairment and Alzheimer's disease: implications for sequence of pathological events in Alzheimer's disease. Brain 2009; 132: 1355-65.

[2] Hardy J, Selkoe DJ. The amyloid hypothesis of Alzheimer's disease: progress and problems on the road to therapeutics. Science 2002; 297: 353-6.

[3] Valk J, Barkhof F, Scheltens P. Magnetic resonance in dementia. 2002, Heidelberg Berlin New York: Springer-Verlag. 353.
[4] Blennow K, de Leon MJ, Zetterberg H. Alzheimer's disease. Lancet 2006; 368: 387-403.
[5] Nordberg A. Amyloid imaging in Alzheimer's disease. Curr Opin Neurol 2007; 20: 398-402.
[6] Klunk WE, Engler H, Nordberg A, *et al.* Imaging brain amyloid in Alzheimer's disease with Pittsburgh Compound-B. Ann Neurol 2004; 55: 306-19.
[7] Choi SR, Golding G, Zhuang Z, *et al.* Preclinical properties of 18F-AV-45: a PET agent for Abeta plaques in the brain. J Nucl Med 2009; 50: 1887-94.
[8] Klunk WE, Lopresti BJ, Ikonomovic MD, *et al.* Binding of the positron emission tomography tracer Pittsburgh compound-B reflects the amount of amyloid-beta in Alzheimer's disease brain but not in transgenic mouse brain. J Neurosci 2005; 25: 10598-606.
[9] Kuntner C, Kesner AL, Bauer M, *et al.* Limitations of small animal PET imaging with [18F]FDDNP and FDG for quantitative studies in a transgenic mouse model of Alzheimer's disease. Mol Imaging Biol 2009; 11: 236-40.
[10] Benveniste H, Einstein G, Kim KR, Hulette C, Johnson GA. Detection of neuritic plaques in Alzheimer's disease by magnetic resonance microscopy. Proc Natl Acad Sci USA 1999; 96: 14079-14084.
[11] Dhenain M, Privat N, Duyckaerts C, Jacobs RE. Senile plaques do not induce susceptibility effects in T2*-weighted MR microscopic images. NMR Biomed 2002; 15: 197-203.
[12] Van Rooden S, Maat-Schieman ML, Nabuurs RJ, *et al.* Cerebral Amyloidosis: Postmortem Detection with Human 7.0-T MR Imaging System. Radiology 2009; 253: 788-796.
[13] Nakada T, Matsuzawa H, Igarashi H, Fujii Y, Kwee IL. In vivo visualization of senile-plaque-like pathology in Alzheimer's disease patients by MR microscopy on a 7T system. J Neuroimaging 2008; 18: 125-9.
[14] Meadowcroft MD, Connor JR, Smith MB, Yang QX. MRI and histological analysis of beta-amyloid plaques in both human Alzheimer's disease and APP/PS1 transgenic mice. J Magn Reson Imaging 2009; 29: 997-1007.
[15] Lee SP, Falangola MF, Nixon RA, Duff K, Helpern JA. Visualization of beta-Amyloid plaques in a transgenic mouse model of Alzheimer's disease using MR microscopy without contrast reagents. Magn Reson Med 2004; 52: 538-544.
[16] Jack CR, Jr., Garwood M, Wengenack TM, *et al.* In vivo visualization of Alzheimer's amyloid plaques by magnetic resonance imaging in transgenic mice without a contrast agent. Magn Reson Med 2004; 52: 1263-1271.
[17] Jack CR, Jr., Wengenack TM, Reyes DA, *et al.* In vivo magnetic resonance microimaging of individual amyloid plaques in Alzheimer's transgenic mice. J Neurosci 2005; 25: 10041-8.
[18] Braakman N, Matysik J, van Duinen SG, *et al.* Longitudinal assessment of Alzheimer's beta-amyloid plaque development in transgenic mice monitored by in vivo magnetic resonance microimaging. J Magn Reson Imaging 2006: 530-536.
[19] Chamberlain R, Reyes D, Curran GL, *et al.* Comparison of amyloid plaque contrast generated by T2-weighted, T2*-weighted, and susceptibility-weighted imaging methods in transgenic mouse models of Alzheimer's disease. Magn Reson Med 2009; 61: 1158-64.
[20] Dhenain M, El Tannir El Tayara N, Wu T-D, *et al.* Characterization of in vivo MRI detectable thalamic amyloid plaques from APP/PS1 mice. Neurobiol Aging 2009; 30: 41-53.
[21] Vanhoutte G, Dewachter I, Borghgraef P, Van Leuven F, Van der Linden A. Noninvasive in vivo MRI detection of neuritic plaques associated with iron in APP[V717I] transgenic mice, a model for Alzheimer's disease. Magn Reson Med 2005; 53: 607-13.
[22] Faber C, Zahneisen B, Tippmann F, Schroeder A, Fahrenholz F. Gradient-echo and CRAZED imaging for minute detection of Alzheimer plaques in an APP(V717I) x ADAM10-dn mouse model. Magn Reson Med 2007; 57: 696-703.
[23] El Tannir El Tayara N, Volk A, Dhenain M, Delatour B. Transverse relaxation time reflects brain amyloidosis in young APP/PS1 transgenic mice. Magn Reson Med 2007; 58: 179-84.
[24] Roberts TP, Mikulis D. Neuro MR: principles. J Magn Reson Imaging 2007; 26: 823-37.
[25] Sobol WT. Magnetic resonance contrast agents. Physical basis of relaxation. Neuroimaging Clin N Am 1994; 4: 27-42.
[26] Bloembergen N. Proton Relaxation Times in Paramagnetic Solutions. J. Chem. Phys. 1957; 27: 572-573
[27] Bloembergen N, Morgan LO. Proton Relaxation Times in Paramagnetic Solutions. Effects of Electron Spin Relaxation. J Chem Phys 1961; 34: 842-850.
[28] Solomon I. Relaxation Processes in a System of Two Spins. Phys Rev 1955; 99: 559-565.
[29] Botta M. Second Coordination Sphere Water Molecules and Relaxivity of Gadolinium(III) Complexes: Implications for MRI Contrast Agents. European Journal of Inorganic Chemistry 2000: 399-407.
[30] Mendonça-Dias MH, Gaggelli E, Lauterbur PC. Paramagnetic contrast agents in nuclear magnetic resonance medical imaging. Sem Nucl Med 1983; 13: 364-376.
[31] Caravan P, Ellison JJ, McMurry TJ, Lauffer RB. Gadolinium(III) Chelates as MRI Contrast Agents: Structure, Dynamics, and Applications. Chem Rev 1999; 99: 2293-352.
[32] Vander Elst L, Roch A, Gillis P, *et al.* Dy-DTPA derivatives as relaxation agents for very high field MRI: the beneficial effect of slow water exchange on the transverse relaxivities. Magn Reson Med 2002; 47: 1121-30.
[33] Wang YX, Hussain SM, Krestin GP. Superparamagnetic iron oxide contrast agents: physicochemical characteristics and applications in MR imaging. Eur Radiol 2001; 11: 2319-31.
[34] Petiet A, Bertrand A, Wiggins C, *et al.* In vivo and post-mortem detection of amyloid plaques with a non-specific gadolinium contrast agent. in Proceedings 17th Scientific Meeting, International Society for Magnetic Resonance in Medicine. 2009. Honolulu: 1090.
[35] Wadghiri YZ, Sigurdsson EM, Wisniewski T, Turnbull DH. Magnetic resonance imaging of amyloid plaques in transgenic mice. Methods Mol Biol 2005; 299: 365-79.
[36] Sigurdsson EM, Wadghiri YZ, Mosconi L, *et al.* A non-toxic ligand for voxel-based MRI analysis of plaques in AD transgenic mice. Neurobiol Aging 2008; 29: 836-47.
[37] Ramakrishnan M, Wengenack TM, Kandimalla KK, *et al.* Selective Contrast Enhancement of Individual Alzheimer's Disease Amyloid Plaques Using a Polyamine and Gd-DOTA Conjugated Antibody Fragment Against Fibrillar Abeta42 for Magnetic Resonance Molecular Imaging. Pharm Res 2008; 25(8): 1861-72.
[38] Poduslo JF, Wengenack TM, Curran GL, *et al.* Molecular targeting of Alzheimer's amyloid plaques for contrast-enhanced magnetic resonance imaging. Neurobiol Dis 2002; 11: 315-29.
[39] Zaim Wadghiri Y, Sigurdsson EM, Sadowski M, *et al.* Detection of Alzheimer's amyloid in transgenic mice using magnetic resonance microimaging. Magn Reson Med 2003; 50: 293-302.
[40] Wadghiri Y, Douadi M, Wisniewski T, Yang J, Utku Y, Kirshenbaum K. Targeting Alzheimer's plaques with Dysprosium based probes. in Proceedings 16th Scientific Meeting, International Society for Magnetic Resonance in Medicine. 2008. Toronto: 255.
[41] Maggio JE, Stimson ER, Ghilardi JR, *et al.* Reversible in vitro growth of Alzheimer disease beta-amyloid plaques by deposition of labeled amyloid peptide. Proc Natl Acad Sci USA 1992; 89: 5462-6.
[42] Trouche SG, Asuni A, Rouland S, *et al.* Antibody response and plasma Abeta1-40 levels in young Microcebus murinus primates immunized with Abeta1-42 and its derivatives. Vaccine 2009; 27: 957-64.
[43] Poduslo JF, Ramakrishnan M, Holasek SS, *et al.* In vivo targeting of antibody fragments to the nervous system for Alzheimer's disease immunotherapy and molecular imaging of amyloid plaques. J Neurochem 2007; 102: 420-33.
[44] Poduslo JF, Curran GL. Polyamine modification increases the permeability of proteins at the blood-nerve and blood-brain barriers. J Neurochem 1996; 66: 1599-609.
[45] Choi JJ, Pernot M, Small SA, Konofagou EE. Noninvasive, transcranial and localized opening of the blood-brain barrier using focused ultrasound in mice. Ultrasound Med Biol 2007; 33: 95-104.
[46] Raymond SB, Treat LH, Dewey JD, McDannold NJ, Hynynen K, Bacskai BJ. Ultrasound enhanced delivery of molecular imaging and therapeutic agents in Alzheimer's disease mouse models. PLoS ONE 2008; 3: e2175.
[47] Howles G, Frinkley K, Qi Y, Nightingale K, Johnson G. Opening the Blood Brain Barrier with Ultrasound for In Vivo Contrast-Enhanced Imaging of the Mouse Brain. in Proceedings 16th Scientific Meeting, International Society for Magnetic Resonance in Medicine 2008. Toronto: 2306.

[48] Bing KF, Howles GP, Qi Y, Palmeri ML, Nightingale KR. Blood-brain barrier (BBB) disruption using a diagnostic ultrasound scanner and Definity in Mice. Ultrasound Med Biol 2009; 35: 1298-308.

[49] Abbott NJ, Romero IA. Transporting therapeutics across the blood-brain barrier. Mol Med Today 1996; 2: 106-13.

[50] Abbott NJ, Ronnback L, Hansson E. Astrocyte-endothelial interactions at the blood-brain barrier. Nat Rev Neurosci 2006; 7: 41-53.

[51] Johnson GA, Cofer GP, Gewalt SL, Hedlund LW. Morphologic phenotyping with MR microscopy: The visible mouse. Radiology 2002; 222: 789-793.

[52] Dhenain M, Delatour B, Walczak C, Volk A. Passive staining: A novel ex vivo MRI protocol to detect amyloid deposits in mouse models of Alzheimer's disease. Magn Reson Med 2006; 55: 687-93.

[53] Kappeler C, Dhenain M, Phan Dinh Tuy F, *et al.* MRI and histological studies of corpus callosal and hippocampal abnormalities linked to doublecortin deficiency. J Comp Neurol 2007; 500: 239-254.

[54] Johnson GA, Cofer GP, Fubara B, Gewalt SL, Hedlund LW, Maronpot RR. Magnetic resonance histology for morphologic phenotyping. J Magn Reson Imaging 2002; 16: 423-9.

[55] Benveniste H, Kim K, Zhang L, Johnson GA. Magnetic resonance microscopy of the C57BL mouse brain. NeuroImage 2000; 11: 601-11.

[56] Petiet A, Hedlund L, Johnson GA. Staining methods for magnetic resonance microscopy of the rat fetus. J Magn Reson Imaging 2007; 25: 1192-8.

[57] Petiet AE, Kaufman MH, Goddeeris MM, Brandenburg J, Elmore SA, Johnson GA. High-resolution magnetic resonance histology of the embryonic and neonatal mouse: a 4D atlas and morphologic database. Proc Natl Acad Sci USA 2008; 105: 12331-6.

[58] Johnson GA, Ali-Sharief A, Badea A, *et al.* High-throughput morphologic phenotyping of the mouse brain with magnetic resonance histology. Neuroimage 2007; 37: 82-9.

[59] D'Arceuil HE, Westmoreland S, de Crespigny AJ. An approach to high resolution diffusion tensor imaging in fixed primate brain. Neuroimage 2007; 35: 553-65.

[60] D'Arceuil H, Liu C, Levitt P, Thompson B, Kosofsky B, de Crespigny A. Three-dimensional high-resolution diffusion tensor imaging and tractography of the developing rabbit brain. Dev Neurosci 2008; 30: 262-75.

[61] Tweedle MF, Wedeking P, Kumar K. Biodistribution of radiolabeled, formulated gadopentetate, gadoteridol, gadoterate, and gadodiamide in mice and rats. Invest Radiol 1995; 30: 372-80.